JOURNAL OF GUIDANCE, CONTROL, AND DYNAMICS
Vol. 29, No. 2, March–April 2006

Sliding-Mode Control for Integrated Missile Autopilot Guidance

Tal Shima*
RAFAEL Armament Development Authority, Ltd., 31021 Haifa, Israel
Moshe Idan†
Technion—Israel Institute of Technology, 32000 Haifa, Israel
and
Oded M. Golan‡
RAFAEL Armament Development Authority, Ltd., 31021 Haifa, Israel

A sliding-mode controller is derived for an integrated missile autopilot and guidance loop. Motivated by a differential game formulation of the guidance problem, a single sliding surface, defined using the zero-effort miss distance, is used. The performance of the integrated controller is compared with that of two different two-loop designs. The latter use a sliding-mode controller for the inner autopilot loop and different guidance laws in the outer loop: one uses a standard differential game guidance law, and the other employs guidance logic based on the sliding-mode approach. To evaluate the performance of the various guidance and control solutions, a two-dimensional nonlinear simulation of the missile lateral dynamics and relative kinematics is used, while assuming first-order dynamics for the target evasive maneuvers. The benefits of the integrated design are studied in several endgame interception engagements. Its superiority is demonstrated especially in severe scenarios where spectral separation between guidance and flight control, implicitly assumed in any two-loop design, is less justified. The results validate the design approach of using the zero-effort miss distance to define the sliding surface.

Nomenclature

A, B, C, G	=	state-space model matrices
a	=	acceleration
D	=	drag force
$f_{(\cdot)}(\cdot)$	=	missile nonlinear aerodynamics function
I	=	moment of inertia
K	=	controller gain
L	=	lift force
$L_{(\cdot)}$	=	lift force derivative
$\mathcal{L}$	=	Lyapunov function
M	=	pitch moment
$M_{(\cdot)}$	=	pitch-moment derivative
m	=	mass
q	=	pitch rate
r	=	range
T	=	engine thrust
t	=	time
t_f	=	final time
t_{go}	=	time to go
V	=	speed
$\boldsymbol{x}$	=	state vector
Z	=	zero-effort miss
z	=	target-missile relative displacement normal to the initial line of sight (LOS)
α	=	angle of attack
γ	=	flight-path angle
Δ	=	modeling error
ΔT	=	maneuver period
$\Delta\phi$	=	maneuver phase
δ	=	canard deflection angle
θ	=	pitch attitude angle
λ	=	angle between the temporary and initial LOS
μ	=	uncertainty control gain
σ	=	sliding variable
τ	=	time constant
Φ	=	transition matrix
ψ	=	time-varying function

Subscripts

a	=	acceleration
bf	=	body coordinates parallel to the inertial frame I
br	=	rotating body-fixed coordinates
G	=	guidance
GC	=	integrated guidance control
I	=	inertial coordinate frame
M	=	missile
MC	=	maneuvering command
N or λ	=	normal to the LOS
q	=	pitching moment
r	=	radial, along the LOS
s	=	servo actuator
T	=	target
0	=	initial values

Superscripts

B	=	body contribution to the aerodynamics force and moment
c	=	command
eq	=	equivalent control
max	=	maximum
$\bar{(\,)}$	=	approximation/model

Presented as Paper 2004-4884 at the Guidance Navigation and Control Conference, Providence, RI, 16–19 August 2004; received 6 December 2004; revision received 4 May 2005; accepted for publication 6 May 2005.

*System Engineer; currently National Research Council Visiting Scientist, Air Vehicles Directorate, Air Force Research Laboratories, Room 304, Building 146, Wright–Patterson AFB, OH 45433; shima_tal@yahoo.com. Senior Member AIAA.

†Associate Professor, Faculty of Aerospace Engineering; moshe.idan@technion.ac.il. Associate Fellow AIAA.

‡Chief Systems Engineer, P.O. Box 2250, Department 35; odedgol@rafael.co.il. Senior Member AIAA.

I. Introduction

FLIGHT control and guidance loops of interceptor missiles are usually assumed to be spectrally separated. Thus, a hierarchical

design approach is commonly used, in which an inner-loop autopilot is constructed to follow acceleration commands issued by the outer-loop guidance algorithm. The guidance law is designed based on a low-order approximation of the autopilot dynamics. Such a practice allows simple, lower-order, analysis of each of the design cycles and enables conventional gain scheduling.[1] However, close to interception spectral separation might not be valid because of rapid changes in the relative geometry. This can cause instability and, consequently, unacceptable miss distances.

A possible development in future interceptors is the requirement for very small miss distances in order to reduce warheads' size (and consequently their lethal radii) without affecting the interception effectiveness. The integrated flight control and guidance law design can enhance the endgame performance of the interceptor by accounting for the coupling between the control and guidance dynamics. The integrated design that provides synergism between the two control components can also postpone the endgame instability. In such a design, the entire guidance and control loop is stated as a solution to a finite horizon control problem, instead of the common approach treating the inner autopilot loop as an unrealistically infinite horizon one. The integrated design also allows for a more effective use of the information on the missile states in the guidance problem formulation, as opposed to using only the missile acceleration data in separated guidance loop designs.

The potential for improved performance of an integrated autopilot-guidance design has motivated a considerable research effort in this area during the last decade. In Ref. 2, a game theoretic approach was used for the design of an integrated autopilot-guidance linear controller, which minimizes the final miss distance and control energy under worst-case target maneuvers and measurements uncertainty. The feedback linearization method[3] in conjunction with the linear-quadratic-regulator approach were used in Ref. 4 for the design of an integrated controller. A similar approach was used in Ref. 5 in a finite horizon problem setting. In the latter, numerical nonlinear solution techniques have been employed requiring an online solution of a two-point boundary-value problem. In Ref. 6, a state-dependent Riccati differential equation approach was used for designing the integrated controller. Using a six-degrees-of-freedom simulation, it was shown that the integrated controller provides improved miss distance statistics compared to the conventional two-loop design practice.

The sliding-mode-control (SMC) methodology[7] is an intuitive and simple robust control technique, addressing highly nonlinear systems with large modeling errors. SMC was successfully used in the design of controllers for the autopilot and guidance loops, as will be outlined in the next section. The main contribution of the current work is in the derivation of an integrated autopilot-guidance controller using the SMC approach, utilizing the zero-effort miss distance as its single sliding surface.

A difficulty arises when applying SMC to nonminimum phase (NMP) systems because of the implicit plant inversion of the method. Different ways were suggested to treat NMP plants, for example, in Ref. 8, by introducing dynamic sliding manifolds. In this paper we examine a canard control configuration that has minimum phase acceleration dynamics. This type of airframe is often used in short-range air-to-air missiles because of its high agility compared to a tail control configuration.

The remainder of this paper is organized as follows: In the next section, the methodology of designing autopilot and guidance controllers using the SMC approach is discussed. Then, the nonlinear engagement kinematics and missile dynamics equations are reviewed along with the simplified models used for the autopilot and guidance law designs. This is followed by the synthesis of an integrated autopilot-guidance control law, along with two different conventional two-loop designs presented for comparison. A performance analysis is then presented followed by concluding remarks. The system zero dynamics are analyzed in the Appendix.

II. Methodology

In this paper the SMC methodology is used to design guidance and control algorithms for the endgame phase of an interception task. In this section, the SMC methodology and its previous use in missile guidance and control are first briefly reviewed. Then we address the central aspect of this work: the proper definition of the sliding surface that dictates the SMC design.

A. SMC—Brief Review

The SMC methodology is described in many papers and textbooks including Refs. 7 and 9 and will only briefly be reviewed in this section. SMC is a robust control design approach enabling to maintain stability and performance in the presence of modeling errors. Simplified controllers are obtained using SMC by converting a tracking problem of an nth order dynamical system into a first-order stabilization problem. This approach leads to satisfactory performance in the presence of bounded but otherwise arbitrary parameter inaccuracies and model uncertainties. This is achieved by large magnitude, often high-frequency, control activity that can be at odds with excitation of neglected high-frequency dynamics. To overcome this behavior, the design procedure involves tradeoffs between modeling and performance that are quantified in a simple and intuitive fashion.

The SMC design is performed around a sliding surface or manifold, commonly denoted by $\sigma = 0$, where the sliding variable σ is a function of the system tracking error and possibly its derivatives. The number of derivatives used to define the sliding surface is dictated by the relative degree of the system. The sliding surface is defined so that if the tracking error is confined to that surface this error will decay to zero with desired dynamics. The problem is to drive the scalar quantity defining the sliding surface to zero and maintain it there, ultimately achieving exact tracking. The control action required for this task, obtained by imposing $\dot{\sigma} = 0$ once on the surface, is denoted as the *equivalent control*. When the system response is confined to the sliding surface, it is said that the system is in a sliding mode.

Erroneous equivalent control values can be obtained as a result of system uncertainties and disturbances. To accommodate the resulting departures from the sliding surface, the equivalent controller is augmented by a second component, sometimes referred to as the *uncertainty controller*, the goal of which is to drive the system to the sliding surface in finite time, while ensuring closed-loop stability. The control laws that satisfy the stability requirement, while assuming only the knowledge of the uncertainty bounds, are usually discontinuous across the sliding surface. This discontinuity can cause high-frequency control chattering. Although in some applications chattering might be acceptable, it is often required to limit the control activity even by compromising closed-loop performance. This is achieved by smoothing the discontinuous components of the uncertainty controller or by introducing a boundary layer around the sliding surface.

The SMC design methodology entails three major steps: 1) selection of a sliding surface $\sigma = 0$ (or surfaces in a multi-input/multi-output problem) to ensure stable desired dynamic characteristics of the system once in the sliding mode; 2) computation of the equivalent control to impose $\dot{\sigma} = 0$ once on the sliding surface, while using an approximate model of the system dynamics; and 3) choosing an uncertainty controller to ensure stability and finite time convergence to the surface when $\sigma \neq 0$.

B. SMC for Missile Autopilot and Guidance

The SMC methodology can be used to construct missile autopilot and guidance algorithms. In Ref. 10, a method was introduced for optimally selecting a time-varying sliding surface for a recursive linear time-varying dynamics approximation of nonlinear system dynamics. The method was used to design an autopilot that optimally follows a given acceleration command. The sliding surface was composed of the angle of attack, pitch rate, and velocity errors. A high-order SMC for a robust missile autopilot design was presented in Ref. 11. The design was based on the relative degrees of the plant and actuator dynamics, whereas the controller robustness was aimed at addressing uncertainties in the nonlinear model for these dynamics. A multi-input/multi-output problem was treated in Ref. 12 resulting in multiple sliding manifolds. A 180-deg heading

reversal maneuver was sought while using different manifolds for different stages of the maneuver. The goal was to cope with the varying missile dynamics resulting from the varying flight conditions.

A missile guidance law in the class of proportional navigation (PN), derived using the SMC approach, was proposed in Ref. 13. The sliding surface was selected to be proportional to the line-of-sight (LOS) rate, and the target maneuvers were considered as bounded uncertainties. Using numerical simulations, the superiority of the proposed guidance law over the conventional PN was advocated. In Ref. 14 an adaptive sliding-mode guidance law was derived. Using analysis and simulations, robustness to disturbances and parameter perturbations was shown.

A SMC autopilot-guidance controller was recently presented in Ref. 15. It is composed of a two-loop design, using backstepping and high-order SMC methods. In the outer SMC-like guidance loop, a sliding surface that depends on the LOS rate was defined with the missile pitch rate used as a virtual control. The inner loop was designed to robustly enforce the pitch-rate command of the outer loop in the presence of uncertainties. Numerical simulation was used to demonstrate the performance and robustness of the integrated design in tracking an evasive maneuvering target, in the presence of atmospheric disturbances and uncertainty in the plant and actuator dynamics.

C. Zero-Effort Miss Sliding Surface

The selection of a sliding surface is a central part of the sliding-mode controller design process. As just mentioned, the LOS rate is commonly used to define the sliding surface because the underlying physical principle to be sought is clear: attaining a collision triangle. If the speeds of both the interceptor and the target are constant, and if they are on a collision course, then the LOS between them does not rotate. To attain a collision course, the angular velocity command of the interceptor missile can be chosen to be proportional to the LOS rate, leading to the common PN guidance law.

Another natural candidate for defining the sliding surface is the well-known zero-effort miss distance[16] (ZEM) commonly used in advanced optimal control and differential game formulations of the guidance problem. In a one-sided optimal control optimization problem it has the physical meaning of being the miss distance, if from the current time onwards the interceptor does not apply controls and the target performs the expected maneuver. In a two-sided differential game problem, ZEM is the miss distance, if from the current time onwards both players do not apply controls. This scalar variable is obtained from the homogenous solution of the associated engagement equations of motion. Generally, the ZEM depends on the LOS rate and on the missile and target maneuvers. It can also depend on additional terms stemming from varying speeds of both adversaries.[17]

Using the differential game-based ZEM to define the sliding surface has several advantages. First, if the system response is maintained on the sliding surface, it provides zero miss distance. Once on the surface, no control action is needed to ensure interception in the nominal case with perfect modeling, as long as the target does not issue maneuvering commands. In addition, it reduces the n-dimensional guidance problem to a scalar one, with a dynamic equation that in the nominal case depends only on the system inputs.[18] Therefore, ZEM is chosen to define the sliding surface for the separated guidance and integrated autopilot-guidance designs.

III. Model Derivation

A skid-to-turn cruciform canard controlled missile, which is roll stabilized, is considered. The motion of such a missile can be separated into two perpendicular channels. During the end-game the missile is assumed to fly close to a collision course and the guidance and control problem can be treated as planar in each of these channels. We first present the full nonlinear kinematics and dynamics equations of the interception problem, which will serve for the synthesis and analysis of the nonlinear sliding mode guidance and control designs presented in the sequel. Then, linearized equations will be derived, which will serve as the basis for the selection of the various sliding surfaces.

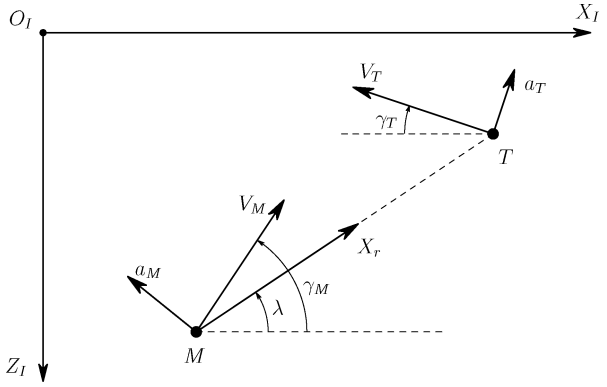

Fig. 1 Planar engagement geometry.

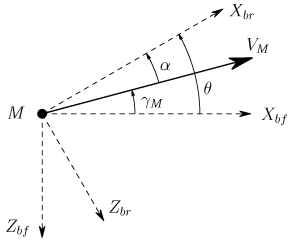

Fig. 2 Missile coordinate systems.

A. Nonlinear Kinematics and Dynamics

1. Engagement Kinematics

In Fig. 1 a schematic view of the planar endgame geometry is shown, where $X_I - O_I - Z_I$ is a Cartesian inertial reference frame. We denote the missile and target by the subscripts M and T, respectively. The speed, normal acceleration, and flight-path angles are denoted by V, a, and γ, respectively; the range between the adversaries is r, and λ is the angle between the LOS and its initial direction.

Neglecting the gravitational force, the engagement kinematics, expressed in a polar coordinate system (r, λ) attached to the missile, is

$$\dot{r} = V_r \tag{1a}$$

$$\dot{\lambda} = V_\lambda / r \tag{1b}$$

where the closing speed V_r is

$$V_r = -[V_M \cos(\gamma_M - \lambda) + V_T \cos(\gamma_T + \lambda)] \tag{2}$$

and the speed perpendicular to the LOS is

$$V_\lambda = -V_M \sin(\gamma_M - \lambda) + V_T \sin(\gamma_T + \lambda) \tag{3}$$

We approximate the time to go t_{go} that will be used in further derivations by

$$t_{\text{go}} = -r / V_r \tag{4}$$

2. Target and Missile Dynamics

During the endgame, the target is assumed to move at a constant speed. In addition we assume first-order lateral maneuver dynamics. This is expressed by

$$\dot{a}_T = \left(a_T^c - a_T\right) \big/ \tau_T \tag{5a}$$

$$\dot{\gamma}_T = a_T / V_T \tag{5b}$$

where τ_T is the time constant of the target dynamics and a_T^c is the maneuver command.

The missile planar dynamics are expressed using the coordinate systems presented in Fig. 2. Here, $X_{\text{br}} - M - Z_{\text{br}}$ is a rotating body-fixed coordinate frame with the X_{br} axis aligned with the

missile's longitudinal axis; $X_{\text{bf}} - M - Z_{\text{bf}}$ is parallel to the inertial frame $X_I - O_I - Z_I$, with its origin attached to the missile center of gravity.

Let α and θ denote the missile's angle of attack and its pitch attitude angle, respectively. Then, the following relation holds:

$$\theta = \alpha + \gamma_M \tag{6}$$

Using the preceding definitions, the planar missile dynamics can be expressed as

$$\dot{V}_M = [T\cos\alpha - D(\alpha,\delta)]/m \tag{7a}$$

$$\dot{\alpha} = q - [T\sin\alpha + L(\alpha,\delta)]/(mV_M) \tag{7b}$$

$$\dot{q} = M(\alpha, q, \delta)/I \tag{7c}$$

$$\dot{\theta} = q \tag{7d}$$

$$\dot{\delta} = (\delta^c - \delta)/\tau_s \tag{7e}$$

where q is the missile pitch rate; m and I are its mass and moment of inertia, respectively; δ is the deflection angle of a canard controlled by a servo actuator represented by a first-order dynamics model with a time constant τ_s; M is the pitch moment acting on the missile; T is the engine thrust that is aligned with X_{br} axis; and L and D are, respectively, the lift and drag forces. The aerodynamic forces and moments are nonlinear, partly unknown functions of the related variables, in particular α, δ, and q. It is assumed that during the endgame the missile has no thrust, and its speed variation is negligible. Hence, the model in Eqs. (7) is reduced to a fourth-order model given by

$$\dot{\alpha} = q - L(\alpha,\delta)/(mV_M) \tag{8a}$$

$$\dot{q} = M(\alpha, q, \delta)/I \tag{8b}$$

$$\dot{\theta} = q \tag{8c}$$

$$\dot{\delta} = (\delta^c - \delta)/\tau_s \tag{8d}$$

B. Linearized Kinematics and Dynamics

Because of the complexity of the preceding nonlinear models, the definition of the sliding surfaces in the various SMC guidance and control designs will be based on simplified kinematics and dynamics models. We will assume that during the endgame the missile and target deviations from the collision triangle are small. Hence, linearization of the endgame kinematics can be performed around the initial LOS.[16] For the control problem we will use the approximate short-period linearized equations of motion.[1]

1. *Engagement Kinematics*

The linearized endgame kinematics used for the decoupled guidance law design is depicted in Fig. 3, where the X axis is aligned with the initial LOS. With the assumption that during the endgame the speeds of the missile and target are constant, the closing speed V_r is constant, and the interception time, given by $t_f = -r_0/V_r$, can be assumed fixed. Therefore, the time to go of Eq. (4) can be computed as

$$t_{\text{go}} = t_f - t \tag{9}$$

The state vector of the linearized guidance problem is defined by

$$\boldsymbol{x}_G = [z \quad \dot{z} \quad a_{\text{TN}} \quad a_{\text{MN}}]^T \tag{10}$$

where z is the relative displacement between the target and the missile normal to the initial LOS direction. The target and missile accelerations normal to the LOS are denoted by a_{TN} and a_{MN}, respectively, and, under the linearization assumption, satisfy

$$a_{\text{MN}} \approx a_M \cos(\gamma_{M0} - \lambda_0) \tag{11}$$

$$a_{\text{TN}} \approx a_T \cos(\gamma_{T0} + \lambda_0) \tag{12}$$

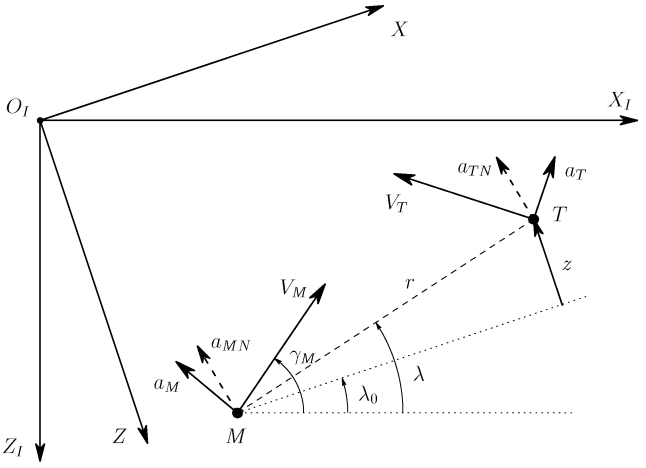

Fig. 3 Linearized endgame kinematics.

where the subscript 0 denotes the initial value around which linearization has been performed.

For nonintegrated guidance law designs, we assume that the closed-loop maneuver dynamics of the missile can be approximated by an equivalent first-order system with a time constant τ_M. Therefore, the equations of relative motion normal to the initial LOS are expressed by

$$\dot{\boldsymbol{x}}_G = A_G\boldsymbol{x}_G + B_G a^c_{\text{MN}} + G_G a^c_{\text{TN}} \tag{13}$$

where

$$A_G = \begin{bmatrix} A_{G11} & A_{G12} \\ [0]_{1\times 3} & -1/\tau_M \end{bmatrix}, \qquad A_{G11} = \begin{bmatrix} 0 & 1 & 0 \\ 0 & 0 & 1 \\ 0 & 0 & -1/\tau_T \end{bmatrix}$$

$$A_{G12} = \begin{bmatrix} 0 \\ -1 \\ 0 \end{bmatrix} \tag{14}$$

$$B_G = \begin{bmatrix} 0 \\ 0 \\ 0 \\ 1/\tau_M \end{bmatrix}, \qquad G_G = \begin{bmatrix} 0 \\ 0 \\ 1/\tau_T \\ 0 \end{bmatrix} \tag{15}$$

and a^c_{TN} and a^c_{MN} are, respectively, the target and missile acceleration commands normal to the initial LOS. In Eq. (14) and hereafter, [0] denotes a matrix of zeros with appropriate dimensions.

2. *Missile Dynamics*

The linearized actuator and short-period missile dynamics, assuming constant speed, are expressed using the state-space vector

$$\boldsymbol{x}_M = [\alpha \quad q \quad \delta]^T \tag{16}$$

Following Eqs. (8), these dynamics are given by

$$\dot{\boldsymbol{x}}_M = A_M\boldsymbol{x}_M + B_M\delta^c \tag{17}$$

where

$$A_M = \begin{bmatrix} -L_\alpha/V_M & 1 & -L_\delta/V_M \\ M_\alpha & M_q & M_\delta \\ 0 & 0 & -1/\tau_s \end{bmatrix}, \qquad B_M = \begin{bmatrix} 0 \\ 0 \\ 1/\tau_s \end{bmatrix} \tag{18}$$

and $L_{(\cdot)}$ and $M_{(\cdot)}$ denote the dimensional stability and control derivatives of the short-period model.

The missile acceleration normal to the initial LOS, which will serve as the control variable in the outer guidance loop of the two-loop guidance and control designs, is given by

$$a_{\mathrm{MN}} = C_M \boldsymbol{x}_M \tag{19}$$

where

$$C_M = [L_\alpha \quad 0 \quad L_\delta]\cos(\gamma_{M0} - \lambda_0) \tag{20}$$

3. Integrated Dynamics

The state vector of the integrated autopilot-guidance problem is defined by

$$\boldsymbol{x}_{\mathrm{GC}} = [z \quad \dot{z} \quad a_{\mathrm{TN}} \quad \alpha \quad q \quad \delta]^T \tag{21}$$

The equations of motion for this case are

$$\dot{\boldsymbol{x}}_{\mathrm{GC}} = A_{\mathrm{GC}}\boldsymbol{x}_{\mathrm{GC}} + B_{\mathrm{GC}}\delta^c + G_{\mathrm{GC}}a^c_{\mathrm{TN}} \tag{22}$$

where

$$A_{\mathrm{GC}} = \begin{bmatrix} A_{G11} & A_{12} \\ [0]_{3\times 3} & A_M \end{bmatrix}, \qquad A_{12} = \begin{bmatrix} [0]_{1\times 3} \\ -C_M \\ [0]_{1\times 3} \end{bmatrix} \tag{23}$$

$$B_{\mathrm{GC}} = [[0]_{1\times 5} \quad 1/\tau_s]^T, \qquad G_{\mathrm{GC}} = [0 \quad 0 \quad 1/\tau_T \quad 0 \quad 0 \quad 0]^T \tag{24}$$

with A_{G11}, A_M, and C_M already defined in Eqs. (14), (18), and (20), respectively.

C. Zero-Effort Miss

As discussed in Sec. II, ZEM is used in the various SMC solutions considered in this paper. It depends on the interception time (or more precisely on the time to go) and is obtained from the homogenous solution of the equations of motion. Therefore, ZEM depends on the analyzed problem and the related model. For complex nonlinear interception models ZEM cannot be determined analytically. Therefore, in the current work approximate ZEMs are derived for linearized models. Nonetheless, the dynamic characteristics of the ZEMs will be determined using the nonlinear models. This approximation approach will be validated in Sec. V through simulation.

1. ZEM for Guidance

For the separated guidance problem, the governing equations are (13–15). Following Ref. 18, let $\Phi_G(t_f, t)$ be the transition matrix associated with these dynamics. For the investigated time-invariant problem it can be computed as

$$\Phi_G(t_f, t) = \Phi_G(t_{\mathrm{go}}) = \exp(A_G t_{\mathrm{go}}) \tag{25}$$

The sparse structure of A_G allows for an analytical solution of $\Phi_G(t_{\mathrm{go}})$, which is then used to determine the guidance ZEM as

$$Z_G \triangleq C_G\Phi_G(t_{\mathrm{go}})\boldsymbol{x}_G = z + \dot{z}t_{\mathrm{go}} + a_{\mathrm{TN}}\tau_T^2\psi(t_{\mathrm{go}}/\tau_T) - a_{\mathrm{MN}}\tau_M^2\psi(t_{\mathrm{go}}/\tau_M) \tag{26}$$

where

$$C_G = [1 \quad 0 \quad 0 \quad 0] \tag{27}$$

and

$$\psi(\zeta) \triangleq \exp(-\zeta) + \zeta - 1 \tag{28}$$

Alternatively, the first two terms in Eq. (26) can be expressed as a function of the kinematics variables V_r and λ. Specifically, using the assumption of small deviations from a collision triangle, the displacement z normal to the initial LOS can be approximated by

$$z \approx (\lambda - \lambda_0)r \tag{29}$$

Differentiating Eq. (29) with respect to time yields

$$z + \dot{z}t_{\mathrm{go}} = -V_r t_{\mathrm{go}}^2\dot{\lambda} \tag{30}$$

Using this expression, the guidance ZEM of Eq. (26) can be expressed as

$$Z_G = -V_r t_{\mathrm{go}}^2\dot{\lambda} + a_{\mathrm{TN}}\tau_T^2\psi(t_{\mathrm{go}}/\tau_T) - a_{\mathrm{MN}}\tau_M^2\psi(t_{\mathrm{go}}/\tau_M) \tag{31}$$

Note that although $\dot{\lambda}$ and a_{MN} are expected to be available through measurements, the target acceleration a_{TN} must be estimated.

2. ZEM for Integrated Autopilot Guidance

The preceding procedure can now be used to determine the ZEM for the integrated autopilot-guidance dynamics of Eqs. (22–24), leading to

$$Z_{\mathrm{GC}} \triangleq z + \dot{z}t_{\mathrm{go}} + a_{\mathrm{TN}}\tau_T^2\psi(t_{\mathrm{go}}/\tau_T) + \psi_\alpha(t_{\mathrm{go}})\alpha + \psi_q(t_{\mathrm{go}})q + \psi_\delta(t_{\mathrm{go}})\delta \tag{32}$$

where $\psi_\alpha(t_{\mathrm{go}})$, $\psi_q(t_{\mathrm{go}})$, and $\psi_\delta(t_{\mathrm{go}})$ are complicated functions of the system parameters and t_{go} and hence of the kinematics variables. Alternatively, the last three terms of Eq. (32) can be obtained from the numerically computed transition matrix $\Phi_{\mathrm{GC}}(t_{\mathrm{go}})$ associated with A_{GC} of Eq. (23). Using this approach and applying the relationship given in Eq. (30), the ZEM is given by

$$Z_{\mathrm{GC}} = -V_r t_{\mathrm{go}}^2\dot{\lambda} + a_{\mathrm{TN}}\tau_T^2\psi(t_{\mathrm{go}}/\tau_T) + C_{\mathrm{GC}}\Phi_{\mathrm{GC}}(t_{\mathrm{go}})\bar{\boldsymbol{x}}_{\mathrm{GC}} \tag{33}$$

where

$$\Phi_{\mathrm{GC}}(t_{\mathrm{go}}) = \exp(A_{\mathrm{GC}}t_{\mathrm{go}}) \tag{34}$$

$$C_{\mathrm{GC}} = [1 \quad 0 \quad 0 \quad 0 \quad 0 \quad 0] \tag{35}$$

$$\bar{\boldsymbol{x}}_{\mathrm{GC}} = [0 \quad 0 \quad 0 \quad \alpha \quad q \quad \delta]^T \tag{36}$$

IV. Autopilot and Guidance Synthesis

To demonstrate the advantages of the proposed integrated guidance and control solution, two additional designs are presented, in which the guidance and flight control problems are addressed separately. All three designs use the SMC methodology in their various components and use the ZEM in the guidance loop. The first solution, representing the baseline design, couples a differential game law (DGL) with an autopilot designed using the sliding mode approach. This design will be referred to as DGL-SMC in the sequel. Then, in the second solution the former SMC autopilot is commanded by a guidance law constructed using the SMC methodology. This design will be termed SMG-SMC. Finally, the proposed integrated guidance and control solution, SMGC, is presented.

For the synthesis performed in this section and the analysis performed next, we assume that perfect information on the states of the problem is available. Thus, if a state is not measurable, such as the target acceleration a_T, we assume it can be estimated.

A. DGL-SMC Baseline Design

In this baseline design, the DGL is used in the guidance loop. It was derived for the approximate linearized model of the endgame kinematics and first-order target and missile dynamics given by Eqs. (13–15), while assuming bounded target and missile acceleration commands.[19] This guidance law is given by

$$a^c_{\mathrm{MN}} = a^{\max}_{\mathrm{MN}}\mathrm{sgn}(Z_G) \tag{37}$$

where Z_G is the ZEM given by Eq. (31), and a^c_M, acting as a command to the inner-loop autopilot, is given by

$$a^c_M = a^c_{\mathrm{MN}} \Big/ \cos(\gamma_M - \lambda) \tag{38}$$

We assume that during the endgame $|\gamma_M - \lambda| < \pi/2$. Note that $a^{\max}_{\mathrm{MN}}$ relates to $a^{\max}_M$ by the same relation as in Eq. (38).

The missile autopilot is derived using the SMC methodology. We assume that the lift and the aerodynamic pitch moment in Eqs. (8) are comprised of the body and fin contributions. This is modeled by

$$L/m = L_\alpha^B f_1(\alpha) + L_\delta f_2(\alpha+\delta) \tag{39a}$$

$$M/I = M_\alpha^B f_3(\alpha) + M_q q + M_\delta f_4(\alpha+\delta) \tag{39b}$$

where

$$L_\alpha^B = L_\alpha - L_\delta \tag{40a}$$

$$M_\alpha^B = M_\alpha - M_\delta \tag{40b}$$

and $f_i(\cdot)$, $i=1, 2, 3, 4$ are bounded functions expressing the nonlinear aerodynamic characteristics of the missile. The autopilot is designed to control the normal acceleration

$$a_M = L/m \tag{41}$$

with L/m defined in Eq. (39a).

The SMC autopilot is designed using an approximation of the nonlinear model of Eqs. (8), (39), and (40), that is,

$$\dot\alpha = q - \left[\bar L_\alpha^B \bar f_1(\alpha) + \bar L_\delta \bar f_2(\alpha+\delta)\right]/V_M \tag{42a}$$

$$\dot q = \bar M_\alpha^B \bar f_3(\alpha) + \bar M_q q + \bar M_\delta \bar f_4(\alpha+\delta) \tag{42b}$$

$$\dot\delta = (\delta^c - \delta)/\tau_s \tag{42c}$$

and

$$\bar a_M = \bar L_\alpha^B \bar f_1(\alpha) + \bar L_\delta \bar f_2(\alpha+\delta) \tag{43}$$

where $\bar L_{(\cdot)}$, $\bar M_{(\cdot)}$, and $\bar f_i(\cdot)$, $i=1, 2, 3, 4$ are approximations of their respective quantities and functions. It is assumed that the difference between a_M and $\bar a_M$

$$a_M - \bar a_M = \Delta_a \tag{44}$$

is bounded

$$|\Delta_a| \le \bar\Delta_a \tag{45}$$

A canard-controlled missile with normal acceleration measurement is minimum phase. Moreover, the normal acceleration output has a relative degree of one with respect to the actuator command δ^c. Therefore, the SMC sliding surface, $\sigma = 0$, is defined using the variable

$$\sigma = \bar a_M - a_M^c \tag{46}$$

The SMC autopilot is designed using the following Lyapunov function candidate:

$$\mathscr{L} = \tfrac{1}{2}\sigma^2 \tag{47}$$

The time derivative of this Lyapunov function candidate is

$$\dot{\mathscr{L}} = \sigma\dot\sigma = \sigma\left(\dot{\bar a}_M - \dot a_M^c\right) \tag{48}$$

where

$$\dot{\bar a}_M = \left[\bar L_\alpha^B \bar f_1'(\alpha)\right]\dot\alpha + \left[\bar L_\delta \bar f_2'(\alpha+\delta)\right](\dot\alpha + \dot\delta) \tag{49}$$

and $\bar f_i'(\cdot)$, $i=1, 2$ denote the partial derivatives of the functions $\bar f_i(\cdot)$, $i=1, 2$ with respect to their respective arguments. Using the modeling error relation of Eq. (44) in the nonlinear model of Eqs. (8), the state derivatives in Eq. (49) can be expressed as

$$\dot\alpha = q - a_M/V_M = q - (\bar a_M + \Delta_a)/V_M \tag{50a}$$

$$\dot\delta = (\delta^c - \delta)/\tau_s \tag{50b}$$

Substituting Eqs. (50) into (49) leads to

$$\dot{\bar a}_M = K_\alpha[q - (\bar a_M + \Delta_a)/V_M] + K_\delta(\delta^c - \delta) \tag{51}$$

where

$$K_\alpha = \bar L_\alpha^B \bar f_1'(\alpha) + \bar L_\delta \bar f_2'(\alpha+\delta) \tag{52a}$$

$$K_\delta = \bar L_\delta \bar f_2'(\alpha+\delta)/\tau_s \tag{52b}$$

The SMC controller is chosen as

$$\delta^c = \delta^{\text{eq}} - \mu\,\text{sgn}(\sigma)/K_\delta \tag{53}$$

where δ^{eq} is the equivalent controller given by

$$\delta^{\text{eq}} = \delta - (K_\alpha/K_\delta)(q - \bar a_M/V_M) \tag{54}$$

and the second term on the right-hand side of Eq. (53) is the uncertainty controller. With this controller, the derivative of the Lyapunov function candidate becomes

$$\dot{\mathscr{L}} = -\sigma\left[\mu\,\text{sgn}(\sigma) + K_\alpha\Delta_a/V_M + \dot a_M^c\right] \tag{55}$$

Assuming that the derivative of the acceleration command is bounded by

$$\left|\dot a_M^c\right| \le \bar\Delta_{\text{MC}} \tag{56}$$

and using the bound in Eq. (45), the derivative in Eq. (55) can be bounded as

$$\dot{\mathscr{L}} \le -|\sigma|[\mu - |K_\alpha/V_M|\bar\Delta_a - \bar\Delta_{\text{MC}}] \tag{57}$$

Choosing

$$\mu > |K_\alpha/V_M|\bar\Delta_a + \bar\Delta_{\text{MC}} \tag{58}$$

ensures that $\dot{\mathscr{L}}$ is negative definite and that the sliding surface $\sigma = 0$ of Eq. (46) is reached in a finite time. This, in turn, implies that perfect tracking of the commanded acceleration can be attained in a finite time.

To comply with the condition in Eq. (56), the discontinuous guidance command of Eq. (37) is smoothed by a high bandwidth low-pass filter. In addition, to avoid chattering as a result of the discontinuous command in Eq. (53), a boundary-layer approximation of the sign function can be used, thus compromising exact tracking by uniform ultimate boundedness of the tracking error.[9]

B. SMG-SMC Design

The decoupled guidance and control design just presented is modified by redesigning its guidance law using the SMC approach. This is mainly aimed at testing the validity of using the ZEM in defining the guidance sliding surface. The guidance law design is based on the ZEM of Eq. (31). Although the ZEM was computed using a linearized model, the consequent guidance logic, which involves a time derivative of the ZEM, will be determined using the nonlinear model.

As will be evident from the subsequent derivation, the ZEM, which we want to regulate to zero, has a relative degree of one with respect to the guidance control signal a_{MN}^c. Therefore, the variable chosen to define the guidance sliding surface is

$$\sigma_G = Z_G \tag{59}$$

The stability of this SMC guidance law is ensured through the analysis of the following candidate Lyapunov function:

$$\mathscr{L}_G = \tfrac{1}{2}\sigma_G^2 \tag{60}$$

Its time derivative is given by

$$\dot{\mathscr{L}}_G = \sigma_G \dot Z_G \tag{61}$$

where

$$\dot{Z}_G = -(\dot{V}_r t_{\rm go}\dot{\lambda} + 2V_r\dot{t}_{\rm go}\dot{\lambda} + V_r t_{\rm go}\ddot{\lambda})t_{\rm go} + [\dot{a}_{\rm TN}\psi(t_{\rm go}/\tau_T) + a_{\rm TN}\psi'(t_{\rm go}/\tau_T)\dot{t}_{\rm go}]\tau_T^2 - [\dot{a}_{\rm MN}\psi(t_{\rm go}/\tau_M) + a_{\rm MN}\psi'(t_{\rm go}/\tau_M)\dot{t}_{\rm go}]\tau_M^2 \quad (62)$$

In the latter,

$$\psi'\left(\frac{t_{\rm go}}{\tau_T}\right) = \frac{\partial\psi(t_{\rm go}/\tau_T)}{\partial t_{\rm go}} = \frac{t_{\rm go}/\tau_T - \psi(t_{\rm go}/\tau_T)}{\tau_T} \quad (63)$$

with a similar result for $\psi'(t_{\rm go}/\tau_M)$. Based on the constant target and missile speed assumptions and using the engagement kinematics of Eqs. (1–4), the derivatives $\dot{V}_r$, $\ddot{\lambda}$ and $\dot{t}_{\rm go}$ are given by

$$\dot{V}_r = V_\lambda^2/r + a_M\sin(\gamma_M - \lambda) + a_T\sin(\gamma_T + \lambda) \quad (64a)$$

$$\dot{V}_\lambda = -V_\lambda V_r/r - a_M\cos(\gamma_M - \lambda) + a_T\cos(\gamma_T + \lambda) \quad (64b)$$

$$\ddot{\lambda} = \dot{V}_\lambda/r - V_\lambda V_r/r^2 \quad (64c)$$

$$\dot{t}_{\rm go} = -1 + \dot{V}_r r/V_r^2 \quad (64d)$$

The true target and missile dynamics are assumed to be related to the approximate first-order linear models by

$$\dot{a}_{\rm TN} = \left(a_{\rm TN}^c - a_{\rm TN}\right)/\tau_T + \Delta_{\rm aTN} \quad (65a)$$

$$\dot{a}_{\rm MN} = \left(a_{\rm MN}^c - a_{\rm MN}\right)/\tau_M + \Delta_{\rm aMN} \quad (65b)$$

where

$$|\Delta_{\rm aTN}| \le \bar{\Delta}_{\rm aTN} \quad (66a)$$

$$|\Delta_{\rm aMN}| \le \bar{\Delta}_{\rm aMN} \quad (66b)$$

are the bounded target and missile dynamics errors. Substituting Eqs. (63–65) into Eq. (62), after some simplifications, the ZEM time derivative is manipulated to yield

$$\dot{Z}_G = \{V_\lambda + a_{\rm TN}\tau_T[1 - \exp(-t_{\rm go}/\tau_T)] - a_{\rm MN}\tau_M \times[1 - \exp(-t_{\rm go}/\tau_M)]\}\dot{V}_r r/V_r^2 + \tau_T\left(a_{\rm TN}^c + \tau_T\Delta_{\rm aTN}\right)\psi(t_{\rm go}/\tau_T) - \tau_M\left(a_{\rm MN}^c + \tau_M\Delta_{\rm aMN}\right)\psi(t_{\rm go}/\tau_M) \quad (67)$$

Note that the first derivative of Z_G yields the maneuver command $a_{\rm MN}^c$, asserting that the relative degree of the ZEM is one. Choosing the control $a_{\rm MN}^c$ as

$$a_{\rm MN}^c = a_{\rm MN}^{\rm eq} + \frac{\mu_G\,\mathrm{sgn}(\sigma_G)}{\tau_M\psi(t_{\rm go}/\tau_M)} \quad (68)$$

where the equivalent control term $a_{\rm MN}^{\rm eq}$ is set to

$$a_{\rm MN}^{\rm eq} = \dot{V}_r r/\left[V_r^2\tau_M\psi(t_{\rm go}/\tau_M)\right]\{V_\lambda + a_{\rm TN}\tau_T[1 - \exp(-t_{\rm go}/\tau_T)] - a_{\rm MN}\tau_M[1 - \exp(-t_{\rm go}/\tau_M)]\} \quad (69)$$

simplifies Eq. (67) to

$$\dot{Z}_G = -\mu_G\,\mathrm{sgn}(\sigma_G) + \tau_T\left(a_{\rm TN}^c + \tau_T\Delta_{\rm aTN}\right)\psi(t_{\rm go}/\tau_T) - \tau_M^2\psi(t_{\rm go}/\tau_M)\Delta_{\rm aMN} \quad (70)$$

The last three unknown terms in Eq. (70) are assumed to be bounded as

$$\left|\tau_T\psi(t_{\rm go}/\tau_T)a_{\rm TN}^c\right| \le \bar{\Delta}_{\rm aTNc} \quad (71a)$$

$$\left|\tau_T^2\psi(t_{\rm go}/\tau_T)\Delta_{\rm aTN}\right| \le \bar{\Delta}_{\rm aTN\tau} \quad (71b)$$

$$\left|\tau_M^2\psi(t_{\rm go}/\tau_M)\Delta_{\rm aMN}\right| \le \bar{\Delta}_{\rm aMN\tau} \quad (71c)$$

Using Eqs. (70) and (71), the time derivative of the guidance Lyapunov function candidate of Eq. (61) can be bounded as

$$\dot{\mathscr{L}}_G \le -|\sigma_G|(\mu_G - \bar{\Delta}_{\rm aTNc} - \bar{\Delta}_{\rm aTN\tau} - \bar{\Delta}_{\rm aMN\tau}) \quad (72)$$

Setting

$$\mu_G > \bar{\Delta}_{\rm aTNc} + \bar{\Delta}_{\rm aTN\tau} + \bar{\Delta}_{\rm aMN\tau} \quad (73)$$

ensures that the guidance sliding surface is attained in finite time. The system response while in sliding mode, that is, its zero dynamics, is investigated in the Appendix. In a realistic noisy interception environment, a boundary layer around the ZEM sliding surface can be employed to provide smooth acceleration commands.

C. SMGC Design

For the integrated guidance and control design, the full nonlinear kinematics and dynamics model is used. The model input is the actuator command δ^c, while the target acceleration command $a_{\rm TN}^c$ is treated as a disturbance. Similar to the SMG-SMC design, the ZEM, this time of Eq. (33), will define the sliding surface. Here again, the relative degree of this ZEM to the input is one, leading to the sliding variable

$$\sigma_{\rm GC} = Z_{\rm GC} \quad (74)$$

The candidate Lyapunov function and its time derivative are

$$\mathscr{L}_{\rm GC} = \tfrac{1}{2}\sigma_{\rm GC}^2 \quad (75)$$

and

$$\dot{\mathscr{L}}_{\rm GC} = \sigma_{\rm GC}\dot{Z}_{\rm GC} \quad (76)$$

Recognizing that the first two terms of Z_G in Eq. (31) and $Z_{\rm GC}$ in Eq. (33) are identical, the results of their differentiation obtained in the SMG case just presented can be used here. Therefore, based on Eq. (33) and the results in Eq. (67),

$$\dot{Z}_{\rm GC} = \{V_\lambda + a_{\rm TN}\tau_T[1 - \exp(-t_{\rm go}/\tau_T)]\}\dot{V}_r r/V_r^2 + \tau_T\left(a_{\rm TN}^c + \tau_T\Delta_{\rm aTN}\right)\psi(t_{\rm go}/\tau_T) - t_{\rm go}a_{\rm MN} + C_{\rm GC}[\Phi'_{\rm GC}(t_{\rm go})\bar{\boldsymbol{x}}_{\rm GC}\dot{t}_{\rm go} + \Phi_{\rm GC}(t_{\rm go})\dot{\bar{\boldsymbol{x}}}_{\rm GC}] \quad (77)$$

where $\dot{t}_{\rm go}$ is given in Eq. (64d) and

$$\Phi'_{\rm GC}(t_{\rm go}) = \frac{\partial\Phi_{\rm GC}(t_{\rm go})}{\partial t_{\rm go}} = A_{\rm GC}\Phi_{\rm GC}(t_{\rm go}) \quad (78)$$

The derivatives $\dot{\alpha}$ and $\dot{\delta}$ in the vector $\dot{\bar{\boldsymbol{x}}}_{\rm GC}$ were derived in Eqs. (50). Using the relations in Eqs. (39b) and (42b), $\dot{q}$ is expressed as

$$\dot{q} = \bar{M}_\alpha^B\bar{f}_3(\alpha) + \bar{M}_q q + \bar{M}_\delta\bar{f}_4(\alpha + \delta) + \Delta_q \quad (79)$$

Here Δ_q denotes a bounded error in the pitching-moment equation satisfying

$$|\Delta_q| \le \bar{\Delta}_q \quad (80)$$

Equations (50), (64d), (78), and (79) are used next to manipulate Eq. (77) into

$$\dot{Z}_{\rm GC} = \{V_\lambda + a_{\rm TN}\tau_T[1 - \exp(-t_{\rm go}/\tau_T)] + C_{\rm GC}\Phi_{\rm GC}(t_{\rm go})\bar{\boldsymbol{y}}_{\rm GC}\}\dot{V}_r r/V_r^2 + \Phi_{\rm GC}^{(1,6)}(t_{\rm go})\delta^c/\tau_s + \tau_T\left(a_{\rm TN}^c + \tau_T\Delta_{\rm aTN}\right)\psi(t_{\rm go}/\tau_T) + \Delta_{\rm GC} \quad (81)$$

where $\bar{\boldsymbol{y}}_{\rm GC} = A_{\rm GC}\bar{\boldsymbol{x}}_{\rm GC}$, $\bar{a}_{\rm MN} = -\bar{\boldsymbol{y}}_{\rm GC}(2)$ (minus the second element of $\bar{\boldsymbol{y}}_{\rm GC}$), and $\Phi_{\rm GC}^{(1,6)}(t_{\rm go})$ is the (1,6)th element of the numerically computed transition matrix $\Phi_{\rm GC}(t_{\rm go})$, that is, the complicated function $\psi_\delta(t_{\rm go})$ used in Eq. (32). All of the bounded modeling errors that were introduced to derive Eq. (81) are grouped into the bound $\Delta_{\rm GC}$. Thus,

$$|\Delta_{\rm GC}| \le \bar{\Delta}_{\rm GC} \quad (82)$$

Motivated by Eq. (81), the SMGC controller is defined as

$$\delta^c = \delta^{\text{eq}} - \mu_{\text{GC}}\,\text{sgn}(\sigma_{\text{GC}})\tau_S \Big/ \Phi_{\text{GC}}^{(1,6)}(t_{\text{go}}) \tag{83}$$

where the equivalent control is given by

$$\delta^{\text{eq}} = -\left\{ V_\lambda + a_{\text{TN}}\tau_T\left[1 - \exp\left(\frac{-t_{\text{go}}}{\tau_T}\right)\right] + C_{\text{GC}}\Phi_{\text{GC}}(t_{\text{go}})\bar{y}_{\text{GC}} \right\} \frac{\dot{V}_r r \tau_s}{V_r^2 \Phi_{\text{GC}}^{(1,6)}(t_{\text{go}})} \tag{84}$$

With this definition of the control signal δ^c, the derivative in Eq. (76) can be bounded by

$$\dot{\mathcal{L}}_{\text{GC}} \le -|\sigma_{\text{GC}}|(\mu_{\text{GC}} - \bar{\Delta}_{\text{aTNc}} - \bar{\Delta}_{\text{aTN}\tau} - \bar{\Delta}_{\text{GC}}) \tag{85}$$

By setting

$$\mu_{\text{GC}} > \bar{\Delta}_{\text{aTNc}} + \bar{\Delta}_{\text{aTN}\tau} + \bar{\Delta}_{\text{GC}} \tag{86}$$

the sliding surface $Z_{\text{GC}} = 0$ can be reached in a finite time. The zero dynamics of the system is investigated in the Appendix.

Similar to the autopilot SMC, chattering caused by the discontinuity of the controller in Eq. (83) can be reduced by replacing the sign function by a high-gain linear element with saturation, that is, a boundary layer.

V. Performance Analysis

Performance of the three guidance and control algorithms just developed is investigated in this section via numerical simulations, using the nonlinear kinematics and missile and target dynamics of Eqs. (1), (5), and (8). First, we outline the test scenario and its parameters. Then, we present a qualitative comparison between the three different designs using a sample run. A quantitative comparison of the homing performance, conducted using a Monte Carlo simulation study, is then discussed.

A. Scenario

The generic interceptor model used in this study is based on the missile control example introduced in Ref. 20. It is assumed that the target performs a square-wave evasive maneuver with a period of ΔT and a phase of $\Delta\phi$ relative to the beginning of the simulation. The initial range was chosen as 1000 m. The engagement geometry and trajectories are plotted in Fig. 4 for an example where the missile initial velocity vector is aligned with the initial LOS. The periodic maneuver of the target and consequently that of the missile are evident. In addition, after a transient caused by the initial heading error, the LOS orientation remains almost constant.

In this simulation study the constant missile speed is assumed to be $V_M = 380$ m/s. The canard servo is characterized by a time constant of $\tau_s = 0.02$ s. The missile model parameters are $\bar{L}_\alpha^B = 1190$ m/s^2, $\bar{L}_\delta = 80$ m/s^2, $\bar{M}_\alpha^B = -234$ s^{-2}, $\bar{M}_q = -5$ s^{-1}, $\bar{M}_\delta = 160$ s^{-2}, $a_M^{\max} = 40$ g, and $\tau_M = 0.1$ s. The target parameters are $V_T = 380$ m/s, $a_T^{\max} = 20$ g, $\Delta T = 1$ s, $\Delta\phi \in [0, 1]$ s, and $\tau_T \in [0.05, 0.2]$ s. The approximate inner-loop parameters τ_M and $a_M^{\max}$ were obtained by evaluating the inner-autopilot-loop performance when operating without the guidance loops. The functions $f_i(\,)$, $i = 1, 2, 3, 4$ of the aerodynamic model [see Eqs. (39)] were chosen to be the standard saturation functions

$$\text{sat}(u) = \begin{cases} U_m & U_m < u \\ u & -U_m \le u \le +U_m \\ -U_m & u < -U_m \end{cases} \tag{87}$$

with $U_m = 30$ deg for all i. For the SMGC design, the model functions $\bar{f}_i(\,)$, $i = 1, 2, 3, 4$ were chosen to be identical to those in Eq. (87). However, because the SMC autopilot requires derivatives of those functions with respect to their argument [see Eqs. (49) and (52)], a smooth approximation of Eq. (87) was used in the DGL-SMC and SMG-SMC designs. Note that all three designs have been implemented with a boundary layer around the respective sliding surfaces. In the inner loop of the DGL-SMC and SMG-SMC designs, the width of the boundary layer around the sliding surface of Eq. (46) was chosen as 0.5 m/s^2, whereas no boundary layer was needed in the outer loop of SMG-SMC. The SMGC design used a boundary layer of 5 cm around its sliding surface from Eq. (74).

B. Sample Run Performance

The performance of the various guidance and control designs is first evaluated and compared for a sample run. The target maneuver is characterized by $\tau_T = 0.05$ s and $\Delta\phi = 0.1$ s. The sample run was performed without missile model uncertainties. The missile aerodynamic parameters were chosen to be identical to the model. In Figs. 5–7 the ZEM, missile acceleration, and canard deflection are compared for the three different designs.

The ZEM plotted in Fig. 5 was computed using Eq. (33) for the integrated design and using Eq. (31) for the other two designs. Large initial heading errors cause large initial ZEMs, reduced significantly at the beginning of the scenario for the three designs. Contrary to the two-loop designs, the integrated SMGC solution does not exhibit an overshoot in the ZEM and nearly nullifies it after the transient stage. The overshoot and somewhat oscillatory response of the DGL-SMC and SMG-SMC designs, triggered by the abrupt changes in the target maneuvers, are attributed to the approximate first-order modeling of the inner loop and its consequent effect on the outer-loop performance.

The missile acceleration for the three designs is plotted in Fig. 6, depicting the periodic missile response imposed by the target maneuver. The acceleration profiles of the two-loop designs

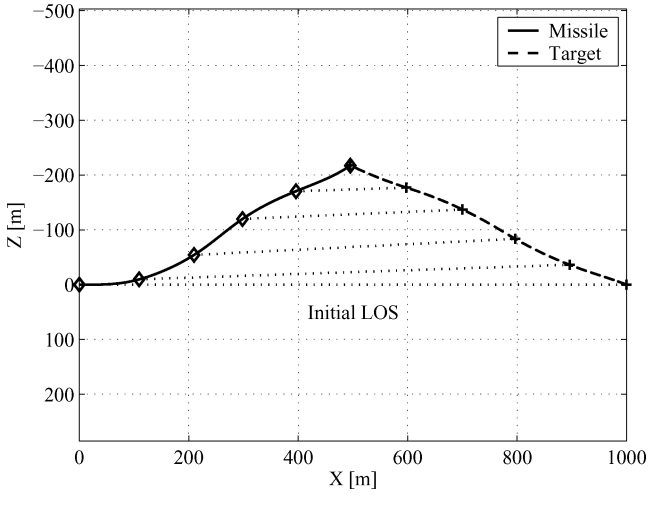

Fig. 4 Sample run engagement trajectories.

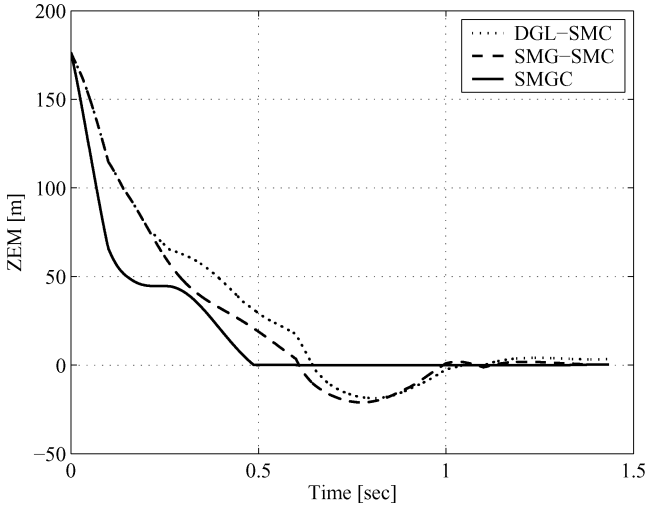

Fig. 5 ZEM comparison for a sample run.

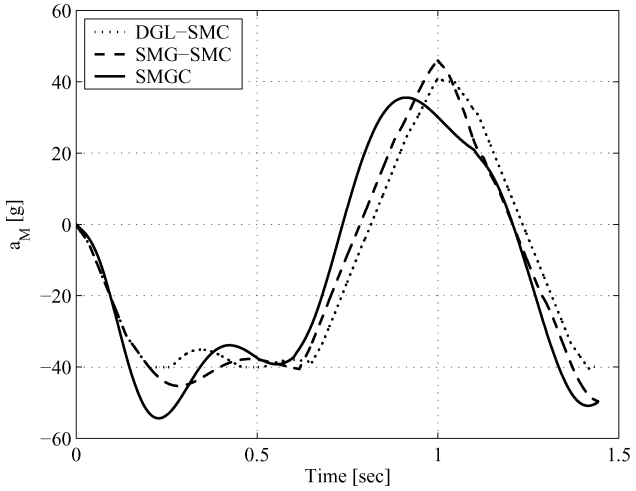

Fig. 6 Acceleration profile comparison for a sample run.

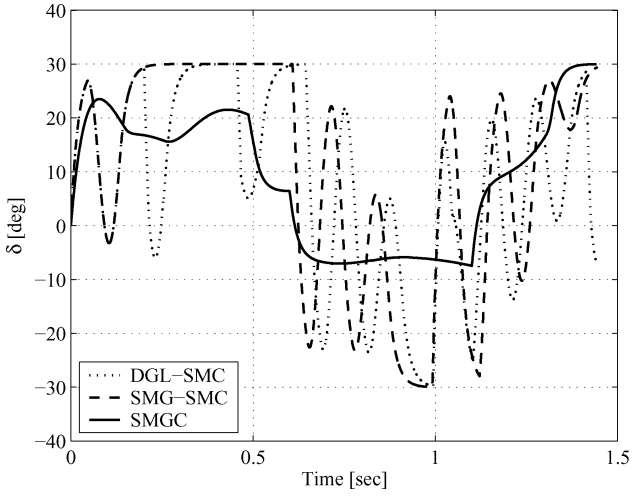

Fig. 7 Canard deflection comparison for a sample run.

are similar throughout the maneuver, whereas that attained by the SMGC solution is similar in magnitude and shape, but is slightly smoother.

The time history of the canard deflection is shown in Fig. 7. During most of the maneuver, very oscillatory and for times saturated canard deflections are observed with the two-loop controllers. Contrary to this behavior, the SMGC controller led to much smoother and smaller deflections, avoiding saturation during most of the maneuver. This demonstrates one of the advantages of the integrated design.

C. Homing Performance

To evaluate and compare the homing performance of the different algorithms, a Monte Carlo simulation study consisting of 100 sample runs for each test point was carried out. In these simulations, for each test case the random variables were chosen to be the target maneuver phase $\Delta\phi$ and the missile aerodynamic parameters (L_α^B, L_δ, M_α^B, M_q, and M_δ). These variables were assumed to be distributed uniformly.

In Fig. 8 the statistics (mean and standard deviation) of the miss distance are plotted for different dynamic capabilities of the target. The aerodynamics coefficients of the missile were varied randomly by $\pm 20\%$ from the model values. It is apparent that the use of the integrated guidance-control algorithm (SMGC) yields superior homing performance, while the two-loop designs (DGL-SMC and SMG-SMC) exhibit similar characteristics. This advantage is amplified for highly maneuverable targets, characterized by small values of τ_T. For such targets the spectral separation between the guidance and flight control is less justified. This demonstrates the main advantage of the integrated design.

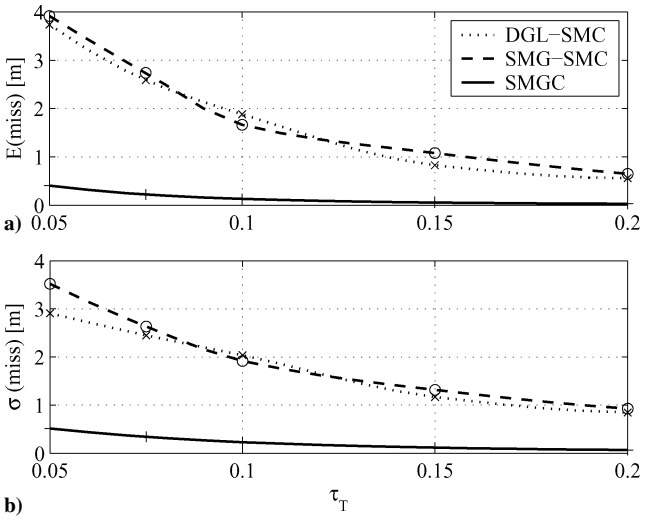

Fig. 8 Homing performance comparison: a) expected miss and b) its standard deviation.

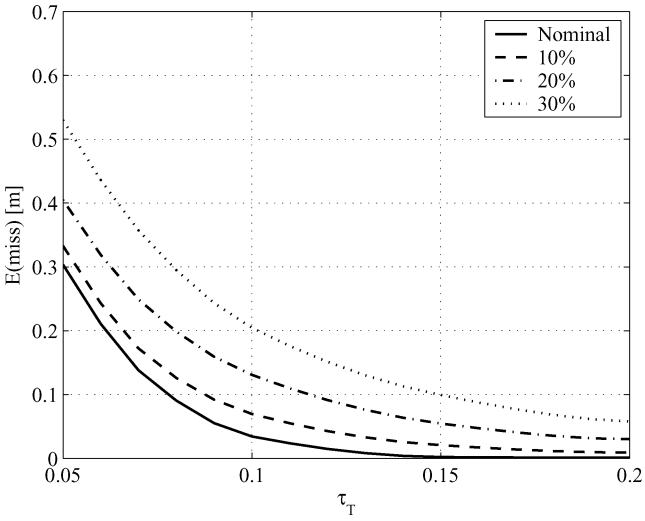

Fig. 9 SMGC sensitivity to modeling errors.

The sensitivity of the integrated design to modeling errors is depicted in Fig. 9. The lower bound on the homing performance is given by the results for the nominal case with no modeling errors. It is apparent that increasing the uncertainty interval has a nonlinear, increasing effect on the homing performance.

The performance of the SMGC controller was evaluated also for varying initial conditions, such as changes in the initial heading angles of the adversaries. It was found that the homing performance was only slightly affected by those changes, resulting in similar results to those presented in Fig. 8.

VI. Conclusions

This paper demonstrates that by using an integrated design for an interceptor missile autopilot and guidance loops, improved performance can be obtained compared to the conventional two-loop design. The advantage of the integrated design is primarily significant in interception scenarios of highly maneuverable targets. In such cases, the inherent instability of the decoupled guidance and control loops near the terminal time is postponed by the integrated design, resulting in reduced miss distances.

The sliding-mode control approach has been used for the derivation of the integrated guidance-control algorithm. The zero-effort miss distance, obtained from a linearized differential game formulation of the interception problem, was used to define the sliding surface of the integrated design. This approach requires the selection of only one time-dependant controller gain, needed to ensure convergence of the missile response to the sliding surface in

the presence of model uncertainties and target maneuvers. Through simulations it was shown that small miss distances can be achieved even in stringent interception scenarios.

The results of this study indicate that the integrated missile autopilot-guidance design, obtained by the sliding-mode approach with zero-effort miss used to define the sliding surface, has the potential of improving interception accuracy in future endgame scenarios against highly maneuverable targets. The enhanced accuracy will enable the use of warheads with smaller kill radius and may even eliminate their need.

Appendix: Zero-Effort Miss Dynamics

In this Appendix we analyze the closed-loop system behavior when it is on the sliding surface, that is, its zero dynamics. In particular, we are interested to verify that while on the sliding surface, that is, when the appropriate ZEM is identically zero, there are no unbounded internal states, and the control input is bounded. For infinite horizon cases, this is ensured when the controlled system, with the sliding variable defined as its output, is minimum phase.[3] However, because the target interception scenario is a finite horizon problem, boundedness of the system signals, while the ZEM is identically zero, will be investigated without actually proving the system being minimum phase.

Guidance ZEM

In the two-loop autopilot and guidance design cases, the states that define the guidance problem are $\boldsymbol{x} = [r \;\; \lambda \;\; a_T \;\; \gamma_T \;\; \gamma_M \;\; a_M]^T$. In this case Z_G of Eq. (31) is used to define the guidance sliding surface. The assumption that the system remains on the sliding surface once it is reached implies that there are no system uncertainties, modeling errors, and unknown disturbances. If this was not the case, the system response would have been moved away from the sliding surface as a result of those uncertainties, contradicting the basic assumption in the current analysis of remaining on the sliding surface.

The equations of motion of the system are given by Eqs. (1) and (5) and by first-order linear missile acceleration dynamics. To analyze the system dynamics on the sliding surface, we introduce the following state transformation $T(\cdot, t)$:

$$y = T(\boldsymbol{x}, t) = [r \quad \lambda \quad a_T \quad \gamma_T \quad \gamma_M \quad Z_G]^T \tag{A1}$$

In the new state variables, the last state Z_G is the sliding variable, treated here as the system output. As shown earlier in Eq. (67), its relative degree is one. Because in this analysis the model uncertainties and disturbances are zero, Eq. (67) simplifies to

$$\dot{Z}_G = \{V_\lambda + a_{\mathrm{TN}}\tau_T[1 - \exp(-t_{\mathrm{go}}/\tau_T)] - a_{\mathrm{MN}}\tau_M \times [1 - \exp(-t_{\mathrm{go}}/\tau_M)]\}\dot{V}_r r \Big/ V_r^2 - a^c_{\mathrm{MN}}\tau_M \psi(t_{\mathrm{go}}/\tau_M) \tag{A2}$$

where a^c_{MN} is the system input.

The differential equations for the first five states in Eq. (A1), while on the sliding surface and hence $a^c_T = 0$, are

$$\dot{r} = V_r \tag{A3a}$$

$$\dot{\lambda} = V_\lambda / r \tag{A3b}$$

$$\dot{a}_T = -a_T/\tau_T \tag{A3c}$$

$$\dot{\gamma}_T = a_T / V_T \tag{A3d}$$

$$\dot{\gamma}_M = a_M / V_M \tag{A3e}$$

where V_r and V_λ are given by Eqs. (2) and (3), respectively.

Based on Eq. (31), while on the sliding surface, the missile acceleration perpendicular to the LOS a_{MN} is given by

$$a_{\mathrm{MN}} = \left[-V_r t_{\mathrm{go}}^2 \dot{\lambda} + a_{\mathrm{TN}}\tau_T^2 \psi(t_{\mathrm{go}}/\tau_T)\right] \Big/ \left[\tau_M^2 \psi(t_{\mathrm{go}}/\tau_M)\right] \tag{A4}$$

and the total missile acceleration a_M relates to a_{MN} by the same relation as in Eq. (38).

The dynamics in Eqs. (A3) are not directly affected by the system input a^c_{MN}. Therefore, the system dynamics for the new states are expressed in the normal form, where $[r \;\; \lambda \;\; a_T \;\; \gamma_T \;\; \gamma_M]^T$ are its internal states.[3] We now examine the boundedness of the internal states in our finite horizon problem, assuming we are on the sliding surface.

The target states are obtained by integrating the homogeneous Eq. (A3c) and then Eq. (A3d). This yields

$$a_T = \exp(-t/\tau_T) a_T(0) \tag{A5}$$

$$\gamma_T = [1 - \exp(-t/\tau_T)] a_T(0)/\tau_T + \gamma_T(0) \tag{A6}$$

which are obviously bounded. Using the relations in Eqs. (2) and (3) together with the assumption that V_M and V_T are constant, we conclude that V_r and V_λ are bounded regardless of γ_T, γ_M, and λ. Consequently, integration of Eq. (A3a) over a finite time interval leads to a bounded r. From Eq. (A3b) we conclude that $\dot{\lambda}$ is bounded, except possibly when $r \to 0$. It is easy to show that $\psi(0) = 0$ and $\psi'(\nu) > 0 \,\forall\, \nu > 0$. Thus we conclude that $\psi(\nu) > 0 \,\forall\, \nu > 0$. Consequently, from Eq. (A4), a_{MN} and a_M are bounded, except for possibly when $r \to 0$.

Based on Eq. (A3e) it also implies that γ_M is bounded for all t except possibly when $r \to 0$.

Now we examine the system response when $r \to 0$. Using Eq. (A4) we obtain that for $r \to 0$ (or equivalently $t_{\mathrm{go}} \to 0$) and while on the sliding surface

$$a_{\mathrm{MN}}(t_{\mathrm{go}} \to 0) \approx -2V_r V_\lambda / r + a_{\mathrm{TN}} \tag{A7}$$

Substituting this result into Eq. (64b), we obtain

$$\dot{V}_\lambda(t_{\mathrm{go}} \to 0) \approx V_r V_\lambda / r \tag{A8}$$

Consequently, using Eq. (A8) in (64c) leads to

$$\ddot{\lambda}(t_{\mathrm{go}} \to 0) \approx 0 \tag{A9}$$

Thus, because Eqs. (64c) and (A9) imply bounded $\ddot{\lambda}$ for all t, we conclude that $\dot{\lambda}$ and λ are bounded. Recalling Eqs. (64a) and (A3b), this implies also boundedness of a_{MN}, a_M, γ_M, and $\dot{V}_r$.

It remains to be shown that the commanded missile acceleration required to remain on the sliding surface is bounded. This commanded acceleration is obtained by setting Eq. (A2) to zero, resulting in

$$a^c_{\mathrm{MN}} = \dot{V}_r r \Big/ \left[V_r^2 \tau_M \psi(t_{\mathrm{go}}/\tau_M)\right] \{V_\lambda + a_{\mathrm{TN}}\tau_T[1 - \exp(-t_{\mathrm{go}}/\tau_T)] - a_{\mathrm{MN}}\tau_M[1 - \exp(-t_{\mathrm{go}}/\tau_M)]\} \tag{A10}$$

All of the terms in the numerator of Eq. (A10) are bounded. We have shown that $\psi(\nu) > 0 \,\forall\, \nu > 0$, and because during the endgame $V_r < 0$ we obtain that the commanded acceleration is also bounded, except possibly when $r \to 0$. Using Eqs. (4) and (A3b), we obtain that for $r \to 0$, while on the sliding surface,

$$a^c_{\mathrm{MN}}(t_{\mathrm{go}} \to 0) \approx 2\tau_M \dot{V}_r \dot{\lambda} \tag{A11}$$

Boundedness of $\dot{\lambda}$ and $\dot{V}_r$ imply also boundedness of the missile acceleration command. This completes the proof that all of the internal states of the guidance problem and the acceleration command, when solved using the SMG approach, are bounded when on the sliding surface $Z_G(t) \equiv 0$.

Integrated ZEM

The states $\boldsymbol{x} = [r \;\; \lambda \;\; a_T \;\; \gamma_T \;\; \gamma_M \;\; \alpha \;\; q \;\; \delta]^T$ define the integrated autopilot-guidance problem. Here, Z_{GC} of Eq. (33) is used to define the sliding surface. The equations of motion of the system are given by Eqs. (1), (5), and (8).

We now introduce the following state transformation $T(\cdot, t)$:

$$y = T(\boldsymbol{x}, t) = [r \quad \lambda \quad a_T \quad \gamma_T \quad \gamma_M \quad \alpha \quad q \quad Z_{\mathrm{GC}}]^T \tag{A12}$$

In the new state variables, the last state Z_{GC} is the sliding variable, treated here as the system output. As shown earlier in Eq. (81), its

relative degree is one. Because in this analysis the model uncertainties and disturbances are zero, Eq. (81) simplifies to

$$\dot{Z}_{\mathrm{GC}} = \{V_\lambda + a_{\mathrm{TN}}\tau_T[1-\exp(-t_{\mathrm{go}}/\tau_T)] + \psi_\alpha(t_{\mathrm{go}})\alpha + \psi_q(t_{\mathrm{go}})q + \psi_\delta(t_{\mathrm{go}})\delta\}\dot{V}_r r\big/V_r^2 + \psi_\delta(t_{\mathrm{go}})\delta^c\big/\tau_s \tag{A13}$$

The differential equations for the first five states in Eq. (A12), while on the sliding surface are given by Eqs. (A3). The nonlinear dynamics equations for α and q are given by Eqs. (8), (39), and (40). The canard deflection angle, while on the sliding surface, can be obtained from Eq. (33):

$$\delta = \left[V_r t_{\mathrm{go}}^2\dot{\lambda} - a_{\mathrm{TN}}\tau_T^2\psi(t_{\mathrm{go}}/\tau_T) - \psi_\alpha(t_{\mathrm{go}})\alpha - \psi_q(t_{\mathrm{go}})q\right]\big/\psi_\delta(t_{\mathrm{go}}) \tag{A14}$$

Note that the first seven states are not directly affected by the system input δ^c. Therefore, the system dynamics for the new states are expressed in the normal form, where $[r\ \ \lambda\ \ a_T\ \ \gamma_T\ \ \gamma_M\ \ \alpha\ \ q]^T$ are its internal states.[3]

We now examine the boundedness of the internal states in our finite horizon problem, assuming we are on the sliding surface $Z_{\mathrm{GC}} = 0$. From Eqs. (8), (39), (40), and (41), we obtain that, because $f_i(\cdot), i = 1, 2, 3, 4$ are bounded functions, the internal missile dynamics states α, q, and the missile acceleration a_M are bounded. The latter implies also boundedness of γ_M. Based on the arguments provided in the preceding subsection, the internal states r, a_T, and γ_T are bounded. In addition, $\dot{\lambda}$ is bounded, except maybe for $r \to 0$. From Eq. (A14), assuming $\psi_\delta(\nu) < 0\,\forall\,\nu > 0$ (this assumption has been verified numerically), we obtain that on the surface the fin deflection angle δ is also bounded, except maybe for $r \to 0$.

Using a series expansion of Φ_{GC} from Eq. (34), we obtain

$$\psi_\alpha(t_{\mathrm{go}} \to 0) \approx -\bar{L}_\alpha\cos(\gamma_{M0}-\lambda_0)t_{\mathrm{go}}^2\big/2 \tag{A15a}$$

$$\psi_q(t_{\mathrm{go}} \to 0) \approx -\bar{L}_\alpha\cos(\gamma_{M0}-\lambda_0)t_{\mathrm{go}}^3\big/6 \tag{A15b}$$

$$\psi_\delta(t_{\mathrm{go}} \to 0) \approx -\bar{L}_\delta\cos(\gamma_{M0}-\lambda_0)t_{\mathrm{go}}^2\big/2 \tag{A15c}$$

Using Eq. (A14), we obtain that for $r \to 0$ (or equivalently $t_{\mathrm{go}} \to 0$) and while on the sliding surface

$$\delta(t_{\mathrm{go}} \to 0) \approx [-2V_r V_\lambda/r + a_{\mathrm{TN}} - \bar{L}_\alpha\alpha\cos(\gamma_{M0}-\lambda_0)]/[\bar{L}_\delta\cos(\gamma_{M0}-\lambda_0)] \tag{A16}$$

Substituting this result into Eq. (64b), we obtain that

$$\dot{V}_\lambda(t_{\mathrm{go}} \to 0) \approx V_r V_\lambda/r + \Delta_{\mathrm{aM}} \tag{A17}$$

where

$$\Delta_{\mathrm{aM}} = \tilde{a}_M\cos(\gamma_{M0}-\lambda_0) - a_M\cos(\gamma_M-\lambda) \tag{A18}$$

and

$$\tilde{a}_M = \bar{L}_\alpha\alpha + \bar{L}_\delta\delta \tag{A19}$$

Because a_M, α, and δ are bounded, then so is Δ_{aM}. Using Eq. (A17) in Eq. (64c) leads to

$$\ddot{\lambda}(t_{\mathrm{go}} \to 0) \approx \Delta_{\mathrm{aM}} \tag{A20}$$

Because we are dealing with a finite-time interception problem, $\dot{\lambda}$ and consequently the internal state λ are bounded.

The commanded fin deflection angle, while on the sliding surface, is obtained by setting Eq. (A13) to zero, resulting in

$$\delta^c = -\dot{V}_r r\tau_s\big/\left[V_r^2\psi_\delta(t_{\mathrm{go}})\right]\{V_\lambda + a_{\mathrm{TN}}\tau_T[1-\exp(-t_{\mathrm{go}}/\tau_T)] + \psi_\alpha(t_{\mathrm{go}})\alpha + \psi_q(t_{\mathrm{go}})q + \psi_\delta(t_{\mathrm{go}})\delta\} \tag{A21}$$

All of the terms in the numerator of Eq. (A21) were shown to be bounded. Similarly to the SMG proof of the preceding section, because in the endgame $V_r < 0$, the fin control command δ^c is bounded except possibly for $t_{\mathrm{go}} \to 0$.

Using Eqs. (4), (A3b), and (A15c), we obtain that for $r \to 0$, while on the sliding surface,

$$\delta^c(t_{\mathrm{go}} \to 0) \approx \frac{2\dot{V}_r\dot{\lambda}\tau_s}{\bar{L}_\delta\cos(\gamma_{M0}-\lambda_0)} \tag{A22}$$

Boundedness of $\dot{\lambda}$ and $\dot{V}_r$ imply also boundedness of the fin deflection command. This completes the proof that all of the internal states of the integrated guidance-control problem and the fin deflection command, when solved using the integrated SMGC approach, are bounded when on the sliding surface $Z_{\mathrm{GC}}(t) \equiv 0$.

References

[1] Blakelock, J. H., *Automatic Control of Aircraft and Missiles*, 2nd ed., Wiley, New York, 1991, Chap. 7.

[2] Lin, C. F., Wang, Q., Speyer, J. L., Evers, J. H., and Cloutier, J. R., "Integrated Estimation, Guidance, and Control System Design Using Game Theoretic Approach," *Proceedings of the American Control Conference*, American Automatic Control Council, Evanston, IL, 1992, pp. 3220–3224.

[3] Khalil, H. K., *Nonlinear Systems*, 3rd ed., Prentice–Hall, Upper Saddle River, NJ, 2002, Chap. 13.

[4] Menon, P. K., and Ohlmeyer, E. J., "Nonlinear Integrated Guidance-Control Laws for Homing Missiles," AIAA Paper 2001-4160, 2001.

[5] Menon, P. K., Sweriduk, G. D., and Ohlmeyer, E. J., "Optimal Fixed-Interval Integrated Guidance-Control Laws for Hit-to-Kill Missiles," AIAA Paper 2003-5579, 2003.

[6] Palumbo, N. F., and Jackson, T. D., "Integrated Missile Guidance and Control: A State Dependent Riccati Differential Equation Approach," *Proceedings of the IEEE International Conference on Control Applications*, Vol. 1, IEEE Press, Piscataway, NJ, 1999, pp. 243–248.

[7] Utkin, V. I., *Sliding Modes in Control and Optimization*, Springer-Verlag, Berlin, 1992.

[8] Shkolnikov, I. A., and Shtessel, Y. B., "Aircraft Nonminimum Phase Control in Dynamic Sliding Manifolds," *Journal of Guidance, Control, and Dynamics*, Vol. 24, No. 3, 2001, pp. 566–572.

[9] Slotine, J.-J. E., and Li, W., *Applied Nonlinear Control*, Prentice–Hall, Upper Saddle River, NJ, 1991, Chap. 7, pp. 276–307.

[10] Salamci, M. U., Özgören, M. K., and Banks, S. P., "Sliding Mode Control with Optimal Sliding Surfaces for Missile Autopilot Design," *Journal of Guidance, Control, and Dynamics*, Vol. 23, No. 4, 2000, pp. 719–727.

[11] Shkolnikov, I., Shtessel, Y. B., Lianos, D., and Thies, A. T., "Robust Missile Autopilot Design via High-Order Sliding Mode Control," AIAA Paper 2000-3968, 2000.

[12] Thukral, A., and Innocenti, M., "A Sliding Mode Missile Pitch Autopilot Synthesis for High Angle of Attack Maneuvering," *IEEE Transactions on Control Systems Technology*, Vol. 6, No. 3, 1998, pp. 359–371.

[13] Moon, J., and Kim, Y., "Design of Missile Guidance Law Via Variable Structure Control," *Journal of Guidance, Control, and Dynamics*, Vol. 24, No. 6, 2001, pp. 659–664.

[14] Xu, W., Mu, C., and Zhou, D., "Adaptive Sliding-Mode Guidance of a Homing Missile," *Journal of Guidance, Control, and Dynamics*, Vol. 22, No. 4, 1999, pp. 589–594.

[15] Shkolnikov, I., Shtessel, Y. B., and Lianos, D., "Integrated Guidance-Control System of a Homing Interceptor: Sliding Mode Approach," AIAA Paper 2001-4218, 2001.

[16] Zarchan, P., *Tactical and Strategic Missile Guidance*, Progress in Astronautics and Aeronautics, Vol. 176, AIAA, Washington, DC, 1997, pp. 27–28.

[17] Shima, T., and Shinar, J., "Time Varying Pursuit Evasion Game Models with Bounded Controls," *Journal of Guidance, Control, and Dynamics*, Vol. 25, No. 3, 2002, pp. 425–432.

[18] Gutman, S., "On Optimal Guidance for Homing Missiles," *Journal of Guidance, Control, and Dynamics*, Vol. 3, No. 4, 1979, pp. 296–300.

[19] Shinar, J., *Solution Techniques for Realistic Pursuit-Evasion Games*, Advances in Control and Dynamic Systems, Vol. 17, Academic Press, New York, 1981, pp. 63–124.

[20] Friedland, B., *Control System Design: An Introduction to State Space Methods*, McGraw–Hill, New York, 1986, pp. 247, 248.